Are Thermoresponsive Microgels Model Systems for Concentrated Colloidal Suspensions? A Rheology and Small-Angle Neutron Scattering Study

Markus Stieger,[†] Jan Skov Pedersen,[‡] Peter Lindner,[§] and Walter Richtering*

Institute of Physical Chemistry, Christian-Albrechts-University of Kiel, Olshausenstr. 40, D-24098 Kiel, Germany, Department of Chemistry, University of Aarhus, Langelandsgade 140, DK-8000 Aarhus C, Denmark, Institute Laue-Langevin, 6 rue Jules Horowitz, BP 156 - 38042 Grenoble Cedex 9, France, and Institute of Physical Chemistry, RWTH Aachen University, Templergraben 59, D-52056 Aachen, Germany

Received February 24, 2004. In Final Form: June 2, 2004

The structure of concentrated temperature-sensitive poly(*N*-isopropylacrylamide) (PNiPAM) microgel suspensions has been investigated employing rheology and small-angle neutron scattering (SANS). A previously described model expression for the particle form factor $P_{inho}(q)$ is extended by a model hard sphere structure factor $S(q)$, and the average radial density profiles $\phi(r)$ are calculated from the amplitude of the form factor $A(q)$ and the structure factor $S(q)$. By this procedure, a direct real space description of the spatial ordering in the neighborhood of a single particle is obtained. The overall particle size and the correlation length ξ of the concentration fluctuations of the internal polymer network decrease with concentration, revealing the increasing compression of the spheres. Thus, the particle form factor $P_{inho}(q)$ of the swollen PNiPAM microgels depends on concentration. The particle−particle interaction potential does not change significantly between 25 and 32 °C. Even approximately 1 K below the lower critical solution temperature (LCST), the experimental scattering intensity distributions $I(q)/c$ are described very well by the hard sphere structure factor when an equivalent hard sphere particle size R_{HS} and volume fraction η_{HS} are used. Microgels with different degrees of cross-linking and particle size resemble true hard sphere behavior up to effective volume fractions of $\phi_{eff} < 0.35$. At higher effective volume fractions $\phi_{eff} > 0.35$ strong deviations from true hard spheres are observed. Interpenetration of the outer, less cross-linked regions of the soft spheres as well as particle compression occurred at higher concentrations. In agreement with this, the equilibrium colloidal phase behavior and rheology also has some features of soft sphere systems. At temperatures well above the LCST, the interaction potential becomes strongly attractive and the collapsed microgel spheres form aggregates consisting of flocculated particles without significant long-range order. Hence, an attractive interaction potential in concentrated suspensions of PNiPAM microgels leads to distinctively different structures as compared to attractive hard sphere colloids. When the peculiar structural properties of the PNiPAM microgels are considered, they can be used as model systems in colloidal science.

I. Introduction

Colloidal suspensions are often used as model systems in soft condensed matter science to study the structure and dynamics of concentrated dispersions. Especially diffusion, crystallization, and rheology of hard sphere suspensions have been thoroughly investigated.[1−5] Model hard sphere suspensions consist of rigid particles dispersed in a Newtonian fluid that interact with a purely repulsive interparticle interaction potential. Among the well-established systems that display hard-sphere-like behavior are dispersions of sterically stabilized colloids. However, the particle−particle interactions of hard spheres can be altered from repulsive to weakly or strongly attractive by changing the solvent and temperature.[6−8] Attraction and phase separation can also be induced via the depletion effect by addition of free nonabsorbing polymer to dispersions of hard spheres.[9]

Colloidal microgels, a further class of dispersions, have attracted interest as model systems for fundamental studies of, for example, the glass transition.[10,11] In contrast to conventional hard sphere dispersions, microgel particles are chemically cross-linked latex spheres that are swollen by a good solvent. The question has been raised whether microgels can be described with well-known hard sphere models or whether the swelling of the particles leads to softness and deformability.[12] The rigidity of a sphere is expected to depend on the cross-linking density.

An even more complex colloidal behavior can be achieved for thermoresponsive microgels, the properties of which can be controlled by external conditions.[13,14] Water-

* To whom correspondence should be addressed at RWTH Aachen University. E-mail: richtering@rwth-aachen.de.

[†] Christian-Albrechts-University of Kiel.

[‡] University of Aarhus.

[§] Institute Laue-Langevin.

(1) Foss, D. R.; Brady, J. F. *J. Rheol.* **2000**, *44*, 629.

(2) Meeker, S. P.; Poon, W. C. K.; Pusey, P. N. *Phys. Rev. E* **1997**, *55*, 5718.

(3) Pusey, P. N.; Segre, P. N.; Behrend, O. P.; Meeker, S. P.; Poon, W. C. K. *Physica A* **1997**, *235*, 1.

(4) Pusey, P. N.; van Megen, W. *Nature* **1986**, *320*, 340.

(5) Derber, S.; Palberg, T.; Schätzel, K.; Vogel, J. *Physica A* **1997**, *235*, 204.

(6) Jansen, J. W.; de Kriuf, C. G.; Vrij, A. *J. Colloid Interface Sci.* **1986**, *114*, 471; **1986**, *114*, 481; **1986**, *114*, 492.

(7) Rouw, P. W.; Woutersen, A. T. J. M.; Ackerson, B. J.; de Kruif, C. G. *Physica A* **1989**, *156*, 876.

(8) Vrij, A.; Penders, M. H. G. M.; Rouw, P. W.; de Kruif, C. G.; Dhont, J. K. G.; Smits, C. S.; Lekkerkerker, H. N. W. *Farady Discuss. Chem. Soc.* **1990**, *90*, 31.

(9) de Hek, H.; Vrij, A. *J. Colloid Interface Sci.* **1981**, *84*, 409.

(10) Bartsch, E.; Kirsch, S.; Lindner, P.; Scherer, T.; Stölken, S. *Ber. Bunsen-*Ges. *Phys. Chem.* **1998**, *11*, 1597.

(11) Eckert, T.; Bartsch, E. *Phys. Rev. Lett.* **2002**, *89*, 125701.

(12) Bartsch, E.; Frenz, V.; Baschnagel, J.; Schärtl, W.; Sillescu, H. *J. Chem. Phys.* **1997**, *106*, 3743.

(13) Schild, H. G. *Prog. Polym. Sci.* **1992**, *17*, 163.

10.1021/la049518x CCC: $27.50
Published on Web 07/16/2004

swellable microgels consisting of poly(*N*-isopropylacrylamide) (PNiPAM) are known to undergo a temperature-induced volume-phase transition when the lower critical solution temperature (LCST) is approached. (In D_2O, the LCST is about 33 °C, slightly higher than in H_2O.[15,16]) At temperatures below the LCST, water is a good solvent and the spheres are highly swollen. At elevated temperatures, the solvent quality changes, and above the LCST, water is a nonsolvent leading to the collapse of the particles. The size of the particle decreases with increasing temperature. Hence, a major advantage of thermoresponsive particles is that the effective volume fraction ϕ_{eff} can easily be controlled by simple temperature changes while the mass concentration c and, thus, the particle number density n is kept constant. In a concentrated suspension, phase separation occurs at temperatures above the LCST. Because the degree of swelling changes with temperature, the rigidity of the particles depends also on temperature.

In a previous study, we investigated the internal structure of PNiPAM microgels in dilute solution using small-angle neutron scattering (SANS), and a model expression for the particle form factor $P_{inho}(q)$ was introduced.[17] The internal structure of the microgel network and the overall particle form were included in the model, and the real space structure was described by radial density profiles. In the swollen state, the polymer segment density of a particle was found to be not homogeneously distributed but gradually decreasing at the surface. Only when the particles are collapsed at temperatures above the LCST the density profiles are described by a box profile like that of homogeneous hard spheres.

Once the internal structure of a microgel particle in dilute solution is known, the interaction between different particles in concentrated suspension can be investigated. Rheology and phase behavior of concentrated PNiPAM microgel suspensions were studied by Senff and Richtering.[18] They were the first to report on the formation of colloidal crystals made of PNiPAM microgels. The relative zero shear viscosity $\eta_{0,rel}$ obtained in the dilute suspension was employed to define an effective volume fraction ϕ_{eff} that is strongly temperature-dependent. It was demonstrated that ϕ_{eff} allows one to obtain temperature-independent master curves over the entire concentration range for rheological properties and the colloidal phase behavior. At $\phi_{eff} < 0.5$, the viscosity data agreed well with that of hard sphere suspensions. At higher effective volume fractions, however, a soft sphere interaction potential was concluded from the experimental phase diagram and the power law concentration dependence of the plateau modulus G_P.

Hellweg et al. determined the structure of colloidal PNiPAM crystals using SANS.[19] A face-centered-cubic lattice was observed. The structure factor $S(q)$ was extracted by dividing the intensity distribution of a concentrated sample $I_{conc}(q)$ (8.5 wt %) by the intensity distribution of a dilute sample $I_{dil}(q)$ (0.85 wt %). They assumed that the particle form factor $P(q)$ is independent of concentration and that the effective volume fraction ϕ_{eff} of the dilute sample is small enough to neglect interparticle correlations [$S(q) = 1$].

Debord and co-workers[20−22] report on the assembly of colloidal PNiPAM crystals with tunable optical properties. They observed by laser scanning confocal microscopy a compression of the soft microgel particles when they are closely packed in the crystal. Obviously, swollen microgel particles are not rigid and show soft sphere behavior at higher concentrations.

Employing thermodynamic perturbation theory combined with static and dynamic light scattering (DLS), Wu et al. have shown that the particle−particle interaction potential alters strongly with temperature.[23] However, in their calculations they did not account for inhomogeneties in the internal particle structure.

In this contribution, we present a study of the structure formation of concentrated suspensions of PNiPAM microgels using rheology and SANS. The following questions are addressed: (a) How does the size of individual microgel particles change with concentration? (b) How can the interaction be described for highly concentrated microgel suspensions at different temperatures? (c) Do highly swollen microgel particles display hard sphere behavior?

For this purpose, the previously described model expression for the particle form factor $P_{inho}(q)$ is extended by a model structure factor $S(q)$ that enables the experimental data to be fitted also at high concentration. We introduce a new approach for calculating the average radial density profiles around a particle from the amplitude of the form factor $P_{inho}(q)$ and the structure factor $S(q)$. By this approach, we obtain a direct description of the ordering in the neighborhood of a particle, which reveals the degree of particle−particle correlations. Concentrated microgel suspensions with different cross-linking densities and particle sizes will be compared at various temperatures. A broad concentration range will be presented covering samples in the dilute and concentrated liquid phase as well as crystalline and glassy samples (0.1−13.9 wt %).

Table 1. Reagent Quantities Employed for the Synthesis of the PNiPAM Microgels[a]

sample M-cross-linker/R_h(25 °C) (mol %/nm)	NiPAM (g)	BIS (g)	SDS (g)	KPS (g)
M-5.5/115	27.167	2.027	0.567	1.138
M-1.4/141	27.555	0.533	0.525	1.012
M-1.5/353	23.188	0.483	0.014	0.962

[a] All syntheses were carried out in 1500 mL of pure water. The sample name represents the resulting cross-linking density given as the molar ratio of BIS to NiPAM in mol % and the hydrodynamic radius at 25 °C in D_2O, R_h(25 °C), in nanometers. The units are omitted in the sample name for clarity.

II. Experimental Part

A. Synthesis of the PNiPAM Microgels. As described previously, the PNiPAM microgels were prepared in an emulsion copolymerization using *N*-isopropylacrylamide (NiPAM), *N*,*N*′-methylenebisacrylamide (BIS), sodium dodecyl sulfate (SDS), and potassium peroxodisulfate (KPS).[17] To adjust the particle radii and the degree of cross-linking, different quantities of the reagents were used and are shown in Table 1. All SDS concentrations were well below the critical micelle concentration. The polymerization was carried out in 1500 mL of pure water under stirring in an inert gas atmosphere at 70 °C for 6 h. After

(14) Saunders, B. R.; Vincent, B. *Adv. Colloid Interface Sci.* **1999**, *80*, 1.
(15) Shirota, H.; Endo, N.; Horie, K. *Chem. Phys.* **1998**, *238*, 487.
(16) Kujawa, P.; Winnik, F. M. *Macromolecules* **2001**, *34*, 4130.
(17) Stieger, M.; Richtering, W.; Pedersen, J. S.; Lindner, P. *J. Chem. Phys.* **2004**, *120*, 6197.
(18) Senff, H.; Richtering, W. *J. Chem. Phys.* **1999**, *111*, 1705.
(19) Hellweg, T.; Dewhurst, C. D.; Brückner, E.; Kratz, K.; Eimer, W. *Colloid Polym. Sci.* **2000**, *278*, 972.
(20) Debord, J. D. *J. Phys. Chem. B* **2000**, *104*, 6327.
(21) Debord, J. D.; Eustis, S.; Debord, S. B.; Lofye, M. T.; Lyon, L. A. *Adv. Mater.* **2002**, *14*, 658.
(22) Debord, S. B.; Lyon, L. A. *J. Phys. Chem. B* **2003**, *107*, 2927.
(23) Wu, J.; Huang, G.; Hu, Z. *Macromolecules* **2003**, *36*, 440.

filtration and extensive dialysis against pure water, the microgel dispersion was freeze-dried. The characterization of the PNiPAM microgels is described elsewhere.[24] It should be noted that the sample name denotes the degree of cross-linking given as the molar ratio of cross-linker to monomer and the hydrodynamic radius in nanometers at 25 °C in heavy water obtained by DLS. For example, the M-5.5/115 microgel exhibits a degree of cross-linking of 5.5 mol % BIS and a hydrodynamic radius of R_h(25 °C) = 115 nm.

B. Experimental Details. SANS experiments were performed at the instrument D11 of the Institute Laue-Langevin (ILL) in Grenoble, France. A neutron wavelength of $\lambda = 6$ Å or $\lambda = 12$ Å with a spread of $\Delta\lambda/\lambda = 9\%$ was employed. The data were collected on a two-dimensional multidetector (64 × 64 elements of 1 × 1 cm^2) and corrected for background and empty cell scattering. Hellma quartz glass cells were used with a sample thickness of 1 mm. Sample−detector distances of 36.7, 10.5, and 2.5 m were used. The incoherent scattering of H_2O was used for absolute calibration according to standard procedures and software available at the ILL ($GRAS_{ans}P$ V. 3.25). H_2O calibration measurements were performed at sample−detector distances of 10.5 and 2.5 m. Further processing of the isotropic data was done by radially averaging to obtain a one-dimensional data set. All experiments were carried out at full contrast using D_2O as the solvent. The concentrations of the samples were in the range of 0.1−13.9 wt %. At higher concentrations, the samples were highly viscous. When filling the sample cells the microgel dispersions were heated giving rise to a significant decrease in viscosity. The samples were cooled to 25.0 °C after filling. By this procedure, microgel dispersions with a high volume fraction could be prepared without shear ordering effects when filling the sample cells.

Rheological properties of the concentrated PNIPAM dispersions were studied using a stress-controlled Bohlin CVO-120 HR rheometer in cone/plate shear geometry (1°/40 mm).

In addition, the effective volume fractions ϕ_{eff} of the microgel suspensions were determined as described previously[18] employing the relative viscosity η_{rel}, which is related to ϕ_{eff} via an expression derived by Batchelor[25] ($\eta_{rel} = 1 + 2.5\phi_{eff} + 5.9\phi_{eff}^2$). The relative viscosity η_{rel} in dilute solution was measured with a computer-controlled Lauda PVS-1/S5 capillary viscometer.

III. Theory and Data Analysis

A detailed description of the model expression for the scattering intensity distribution $I(q)$ of PNiPAM microgels in dilute solution was described previously.[17] The parameter q denotes the magnitude of the momentum transfer $q = 4\pi/\lambda \sin(\theta/2)$, where λ is the neutron wavelength and θ is the scattering angle. The internal and overall structures of the particles in dilute solution were successfully described by the form factor of an inhomogeneous sphere $P_{inho}(q)$. A model structure factor $S(q)$ accounts for particle−particle correlations at finite concentration. A brief summary of the model expression will be given in the following section with special emphasis on the influence of the structure factor $S(q)$ on the intensity distribution $I(q)$. In addition, we describe a new approach for obtaining the average radial density around the center of a particle from the form factor amplitude and the structure factor $S(q)$.

Including both the (normalized) form factor $P(q)$ to describe the structure of a single particle and the structure factor $S(q)$ to account for the interference of scattering from different particles allows the model to describe more concentrated samples, which were studied in the present work. For a suspension of monodisperse centro-symmetric particles the differential scattering cross section $d\sigma(q)/d\Omega$ is given by

$$\frac{d\sigma(q)}{d\Omega} = n\Delta\rho^2 V_{poly}^2 P(q)\, S(q) \qquad (1)$$

In addition to the form factor $P(q)$ and structure factor $S(q)$ of the particles, the number density of the particles n, the difference in scattering length density between the polymer and the solvent $\Delta\rho$, and the volume of polymer in a particle V_{poly} enter the differential scattering cross section $d\sigma(q)/d\Omega$. The difference in scattering length density $\Delta\rho$ which corresponds to the scattering contrast must be calculated for each microgel suspension because of its dependence on the particle composition (fraction of cross-linking molecules) and the temperature-dependent apparent specific density.

For PNiPAM particles, a higher degree of cross-linking density is expected inside the particle than outside according to the polymerization kinetics.[26] The resulting inhomogeneous internal particle structure described by the form factor $P_{inho}(q)$ will be fuzzy rather than sharp. We convolute the radial scattering length density profile of a homogeneous sphere with a Gaussian to get a function with a gradual drop-off in scattering length density. These spheres with a fuzzy surface are described by the modified form factor $P_{inho}(q)$

$$P_{inho}(q) = [A(q)]^2 \quad \text{with}$$
$$A(q) = \frac{3[\sin(qR) - qR\cos(qR)]}{(qR)^3} \exp\left(-\frac{(\sigma_{surf}q)^2}{2}\right) \qquad (2)$$

where $A(q)$ defines the amplitude of the form factor $P_{inho}(q)$. R and σ_{surf} are the two adjustable parameters, representing the radius of the particle where the scattering length density profile decreased to 1/2 the core density and the width of the smeared particle surface, respectively. The inner regions of the microgel that exhibit a higher degree of cross-linking density are described by the radial box profile extending to a radius of about $R_{box} \approx R - 2\sigma_{surf}$. In dilute solution, the profile approaches 0 at $R_{SANS} \approx R + 2\sigma_{surf}$. Therefore, the overall size of the particle is approximated by the dilute solution radius R_{SANS}.

Thus far, the discussion has focused on monodisperse spheres. However, microgel particles may display a polydispersity. A Gaussian function describing the particle size distribution function $D(R, \langle R\rangle, \sigma_{poly})$ is assumed

$$D(R, \langle R\rangle, \sigma_{poly}) = \frac{1}{\sqrt{2\pi\sigma_{poly}^2\langle R\rangle^2}} \exp\left(-\frac{(R - \langle R\rangle)^2}{2\sigma_{poly}^2\langle R\rangle^2}\right) \qquad (3)$$

with $\langle R\rangle$ describing the average particle radius and σ_{poly} denoting the relative particle size polydispersity.

The structure factor $S(q)$ accounts for the interference of scattering from different particles in concentrated suspensions. Because the structure factor $S(q)$ describes the relative particle−particle positions, it provides information about the interaction of the particles. For monodisperse particles that interact with a spherically symmetric hard sphere interaction potential, $S(q)$ is

(24) Stieger, M.; Richtering, W. *Macromolecules* **2003**, *36*, 8811.
(25) Batchelor, G. K. *J. Fluid Mech.* **1997**, *83*, 97.
(26) Wu, X.; Pelton, R. H.; Hamielec, A. E.; Woods, D. R.; McPhee, W. *Colloid Polym. Sci.* **1994**, *272*, 467.

obtained from liquid state theory employing the Percus–Yevick approximation for the closure relation[27]

$$S(q) = \left[1 + \frac{24\eta_{HS}G(2R_{HS}q)}{2R_{HS}q}\right]^{-1} \quad (4)$$

with

$$G(A) = \frac{\alpha(\sin A - A\cos A)}{A^2} + \frac{\beta(2A\sin A + (2 - A^2)\cos A - 2)}{A^3} + \frac{\gamma[-A^4\cos A + 4\{(3A^2 - 6)\cos A + (A^3 - 6A)\sin A + 6\}]}{A^5} \quad (5)$$

and

$$\alpha = \frac{(1 + 2\eta_{HS})^2}{(1 - \eta_{HS})^4} \qquad \beta = \frac{-6\eta_{HS}[1 + (\eta_{HS}/2)]^2}{(1 - \eta_{HS})^4} \qquad \gamma = \frac{\eta_{HS}\alpha}{2} \quad (6)$$

The two adjustable parameters in $S(q)$ are the hard sphere volume fraction η_{HS} and the corresponding hard sphere radius R_{HS}. The structure factor effects can be treated in a simple decoupling approximation when the particle size polydispersity is low. In this case, the structure factor $S(q, \langle R\rangle)$ is calculated for the average size. Including all these factors, the differential scattering cross section can be written:

$$\frac{d\sigma(q)}{d\Omega} = n\Delta\rho^2 S(q, \langle R\rangle)\int_0^\infty D(R, \langle R\rangle, \sigma_{poly}) \times V_{poly}(R)^2\, P_{inho}(q, R)\, dR \quad (7)$$

The structure factor of hard spheres is the most simple that one can think of. It has the further advantage that relatively simple analytical expressions are available for $S(q)$. The highly swollen PNiPAM microgels are quite soft, and, therefore, one might suspect that the hard sphere potential does not work. However, there are numerous examples that it works quite well for other very soft systems, like block copolymer micelles with a highly swollen corona even up to quite high hard sphere volume fractions.[28,29] Thus, we started out with the hard sphere structure factor $S(q)$ in the analysis of the PNiPAM microgels described in the present study, and it turned out that it worked very well. We, therefore, concluded that we did not have sufficient information in our scattering data to allow the use of a structure factor $S(q)$ for a more sophisticated interaction potential. We note that some of the (effective) hard sphere volume fractions η_{HS} that we determine are quite high and in fact outside the expected validity range of the model and the Percus–Yevick approximation. Hence, these volume fractions have to be considered as just an empirical parametrization of the structure factor effects, which are present in our data. Consequently, one has to be careful with a physical interpretation of the values in the high concentration regime.

In addition, scattering contributions arising from fluctuations of the microgel network are included in the model expression as a Lorentzian function

$$I_{fluct}(q) = \frac{I_{fluct}(0)}{1 + \xi^2 q^2} \quad (8)$$

where $I_{fluct}(0)$ is the $q = 0$ limiting intensity and ξ represents the correlation length of the fluctuations, which can be considered to be related to the blob or mesh size. It should be noted that the Lorentzian describes the ensemble average correlations in the polymer network.

Finally, the model expression accounts for instrumental smearing of the experimental SANS data. This work uses the approach of Pedersen et al. and includes a resolution function $R(\langle q\rangle, q)$ in the model.[30] As a result of the finite collimation of the beam, the wavelength spread of the incoming neutrons, and the finite spatial resolution of the detector, a distribution of radiation with scattering vectors q around the nominal scattering vector $\langle q\rangle$ also contribute to smearing. These three contributions can be approximated separately by Gaussian functions. The combined resolution function $R(\langle q\rangle, q)$ describing the distribution of scattering vectors q contributing to the scattering at the setting $\langle q\rangle$ is obtained

$$R(\langle q\rangle, q) = \frac{q}{\sigma_{smear}^2}\exp\left[-\frac{1}{2}\left(q^2 + \frac{\langle q\rangle^2}{\sigma_{smear}^2}\right)\right] I_0\left(\frac{\langle q\rangle q}{\sigma_{smear}^2}\right) \quad (9)$$

where σ_{smear} represents the width of the instrumental smearing and depends on the different instrumental settings and I_0 is a modified first kind and zeroth order Bessel function.[31] This expression includes smearing contributions from wavelength smearing (9% full width at half-maximum), collimation, and detector resolution.

The last factor in the model expression is a constant background $const_{back}$ to account for residual incoherent scattering. After incorporating all contributions, the complete model expression for the intensity distribution can be fitted to the experimental data:

$$I^{mod}(\langle q\rangle) = \int_0^\infty \frac{d\sigma(q)}{d\Omega} R(\langle q\rangle, q)\, dq \quad (10)$$

with

$$\frac{d\sigma(q)}{d\Omega} = n\Delta\rho^2 S(q, \langle R\rangle)\int_0^\infty D(R, \langle R\rangle, \sigma_{poly}) \times V_{poly}(R)^2\, P_{inho}(q, R)\, dR + I_{fluct}(q) + const_{back} \quad (11)$$

We will now describe a new approach for calculating the average radial density distribution $\phi(r)$ around a particle from the scattering amplitude of the particles $A(q)$ and the structure factor $S(q)$ (see eqs 2 and 4). A numerical Fourier transformation of it provides the radial density profile of a single particle.

At very high concentrations, the particles start to overlap. The overlapping volume fraction of the polymer constitutes a homogeneous component ϕ_{homo}, which spans the entire sample. Our work and related studies show

(27) Kinning, D. J.; Thomas, E. L. *Macromolecules* **1984**, *17*, 1712.
(28) Pedersen, J. S.; Svaneborg, C.; Almdal, K.; Hamley, I. W.; Young, R. N. *Macromolecules* **2003**, *36*, 416.
(29) Pedersen, J. S.; Gerstenberg, M. C. *Colloids Surf., A* **2003**, *213*, 175.
(30) Pedersen, J. S.; Posselt, D.; Mortensen, K. *J. Appl. Crystallogr.* **1990**, *23*, 321.
(31) Freltoft, T.; Kjems, J. K.; Sinha, S. K. *Phys. Rev. B* **1986**, *33*, 269.

that this contribution must be considered as part of the solvent.[32] The nonoverlapping volume fraction of polymer can be regarded as an excess component ϕ_{excess}, which accounts for the modulation of the polymer density beyond the homogeneous component. Thus, the apparent polymer volume in the particle $V_{pol} = (\phi_{poly}4\pi R^3)/3$ increases with concentration. The true total polymer volume in a particle was obtained from samples in dilute solution. For higher concentrations, the fraction of polymer in the homogeneous component ϕ_{homo} was calculated and used to correct the measured polymer volume fraction.

The Fourier transform of the structure factor $S(q)$ gives the probability distribution of the centers of the particles $g(r)$. With a homogeneous contribution ϕ_{homo}, only the excess polymer volume fraction ϕ_{excess} is described by $g(r)$. The probability distribution function $g(r)$ is, therefore, normalized to approach ϕ_{excess} at long distances r. The total distribution of excess polymer around the center of a particle can be obtained by convoluting $g(r)$ by the distribution around the center of a single particle and adding the single particle distribution $\phi_{poly}(r)$. The convolution is done by calculating $[S(q) - 1]A(q)$ and performing a numerical Fourier transformation. This gives a function proportional to $g_{poly}(r) - 1$, which is related to the monomers in other particles. This function can easily be normalized, leading to $g_{excess}(r)$, which approaches the excess polymer volume fraction ϕ_{excess} at large distances and is 0 at short distances. When the single particle distribution $\phi_{poly}(r)$ and the homogeneous contribution are added to this function, it gives the average polymer volume fraction distribution $\phi(r)$ around the center of a particle.

IV. Results and Discussion

A. Phase Behavior and Rheological Properties. Concentrated suspensions of the M-1.4/141 microgel form colloidal crystals. The transition from the liquid phase to a colloidal crystal started at an effective volume fraction of $\phi_{eff,f} = 0.70$ as compared to the freezing transition $\phi_f = 0.494$ for hard spheres. The shift of the freezing transition to higher volume fractions indicates a soft sphere interaction potential[33] which became noticeable at sufficient high concentrations.

Concentrated microgel suspensions are shear thinning. We determined the relative zero shear viscosity $\eta_{0,rel}$ for various temperatures and concentrations from the flow curves as described previously.[18] The relative zero shear viscosity $\eta_{0,rel}$ as a function of effective volume fraction ϕ_{eff} for the M-5.5/115 and M-1.4/141 microgel is shown in Figure 1. A line representing $\eta_{0,rel}$ of model hard spheres as provided by Meeker et al.[2] is also plotted. Good agreement of our experimental data with the hard sphere data is obtained up to an effective volume fraction of $\phi_{eff} < 0.35$ for both samples independent of the cross-linking density. At higher volume fractions $\phi_{eff} > 0.35$, strong deviations from hard sphere behavior are observed. The viscosity diverged for both particles at larger ϕ_{eff}. However, the viscosity master curve of the microgel with a higher cross-linking density (M-5.5/115) runs closer to the hard sphere line and exhibits a smaller ϕ_{max} than the less cross-linked M-1.4/141. The Dougherty–Krieger equation[34] $\{\eta_{0,rel} = [(1 - \phi/\phi_{max}]^{-[\eta]\phi_{max}}\}$ describes the viscosity fairly well when $\phi_{eff,f} = 0.70$ was used as ϕ_{max} and the intrinsic viscosity $[\eta] = 2.98$ for the M-1.4/141 sample. It should be noted that the particle size polydispersities σ_{poly}, which were obtained from the SANS scattering profiles in dilute solution, were similar for both microgels.[17] A polydispersity of $\sigma_{poly} = 9.9\%$ for M-5.5/115 and $\sigma_{poly} = 9.7\%$ for M-1.4/141 was found at 25 °C.

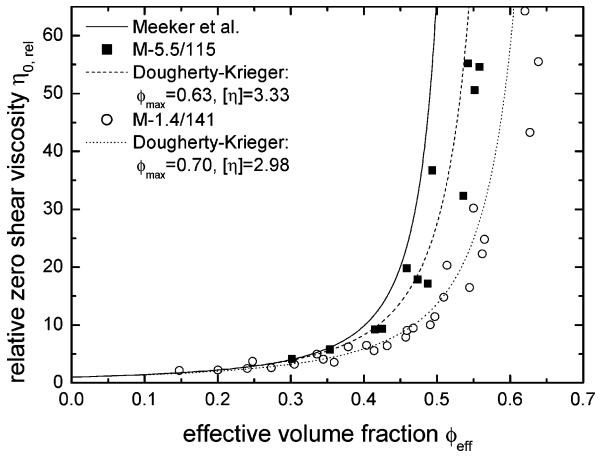

Figure 1. Relative zero shear viscosity, $\eta_{0,rel}$, versus effective volume ϕ_{eff} fraction for the M-5.5/115 and the M-1.4/141 microgels. The solid line represents model hard sphere data provided by Meeker et al.

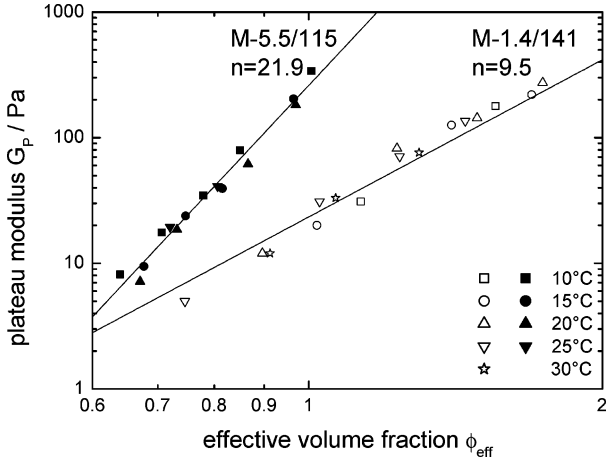

Figure 2. Plateau modulus, G_P, versus effective volume fraction ϕ_{eff} for the M-5.5/115 and the M-1.4/141 microgels. The exponents of the interaction potential n are indicated.

At high concentrations, the samples became viscoelastic and were characterized with low amplitude oscillatory shear experiments. The frequency dependence of the storage modulus G' and loss modulus G'' was investigated, and the frequency-independent plateau modulus G_P was determined. Figure 2 shows the plateau modulus G_P versus the effective volume fraction ϕ_{eff} for two microgels with different cross-linking densities. A master curve was obtained for both samples. G_P can be related to the interaction potential $\psi(r) \propto 1/r^n$ and the pair correlation function using an expression given by Zwanzig and Mountain.[35] When a lattice-like microstructure is assumed where the particles are arranged at well-defined distances, one obtains $G_P \propto (1/r)(\delta^2\psi/\delta r^2)$.[36] We note that Wagner has pointed out that hydrodynamic interactions are neglected in this simple approach.[37] The exponent of the interaction potential n can be related to the slope of the mastercurve via $m = 1 + n/3$, and $n = 21.9$ for M-5.5/115 and $n = 9.5$ for M-1.4/141 were obtained. Thus, both particles reveal soft sphere behavior, but the higher cross-

(32) Sommer, C.; Pedersen, J. S.; Garamus, V. Manuscript in preparation.
(33) Agrawal, R.; Kofke, D. A. *Mol. Phys.* **1995**, *85*, 23.
(34) Krieger, I. M.; Dougherty, T. J. *Trans. Soc. Rheol.* **1959**, *3*, 137.
(35) Zwanzig, R.; Mountain, R. D. *J. Chem. Phys.* **1965**, *43*, 4464.
(36) Buscall, R.; Goodwin, J. W.; Hawkins, M. W.; Ottewill, R. H. *J. Chem. Soc., Faraday Trans. 1* **1982**, *78*, 2889.
(37) Wagner, N. J. *J. Colloid Interface Sci.* **1993**, *161*, 169.

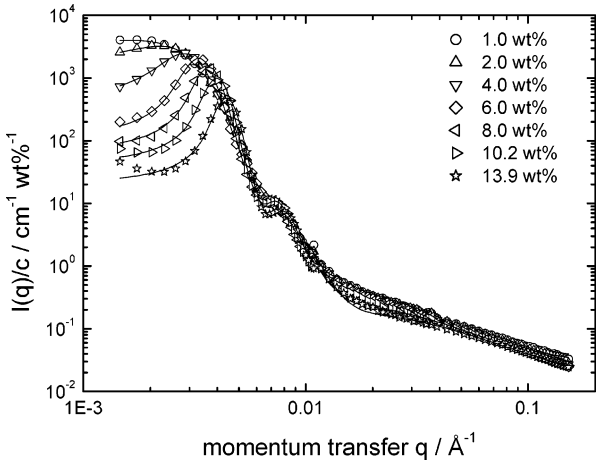

Figure 3. Intensity distribution normalized on concentration, $I(q)/c$, versus momentum transfer q for various concentrations of the M-5.5/115 microgel at 25 °C. The lines represent fits according to eq 10.

linking density of M-5.5/115 leads to a harder interaction potential. A similar influence of the cross-linking density on the interaction potential has been reported by Senff and Richtering.[38]

B. Structural Changes Induced by Temperature and Concentration below the LCST. Figure 3 shows the scattering intensity distribution normalized by the concentration $I(q)/c$ for the M-5.5/115 microgel at 25 °C for different concentrations. The normalized scattering profiles $I(q)/c$ for the same sample but at different temperatures are shown in Figure 4. For the sake of clarity, some of the data sets were multiplied by constant factors as indicated in the diagrams. The lines represent fits according to eq 10. The model describes very well the experimental data at all concentrations and temperatures over the entire q range.

At 25 °C, well below the LCST, the main contribution to the overall scattering intensity $I(q)$ in the low q regime (ca. $0.0014 < q < 0.0055$ Å^{-1}) arises from the structure factor $S(q)$. The evolution of the structure factor peak with concentration can be nicely traced in the low q regime. Already at a mass concentration of $c = 2.0$ wt %, which corresponds to an effective volume fraction of $\phi_{\text{eff}} = 0.20$, a broad maximum in the scattering profile is observed. This indicates that the contribution of the structure factor $S(q)$ to the overall scattering intensity $I(q)$ must be considered and the correlations between different particles cannot be neglected, although the mass concentration is fairly low. With increasing concentration, a decrease of the width of the structure factor peak is observed, which is accompanied by an increase of the peak height. A shift of the structure factor peak toward larger q values with increasing concentrations reveals a decrease of the average particle−particle distance.

The forward scattering intensity $I(q)$ for $q \rightarrow 0$ is reduced by a factor of about 80 when the concentration is raised. At high concentrations (10.2 and 13.9 wt %), $I(q)$ does not reach a constant value for $q \rightarrow 0$ but increases. Those highly concentrated samples reached the glass state. The slowing down of the particle dynamics due to the cage effect in the glass state becomes more efficient with increasing concentration. Eventually, structural relaxation freezes and the structural inhomogeneities of the glassy dispersion can be observed on large length scales. This leads to an increase of $I(q)$ for $q \rightarrow 0$.

(38) Senff, H.; Richtering, W. *Colloid Polym. Sci.* 2000, *278*, 830.

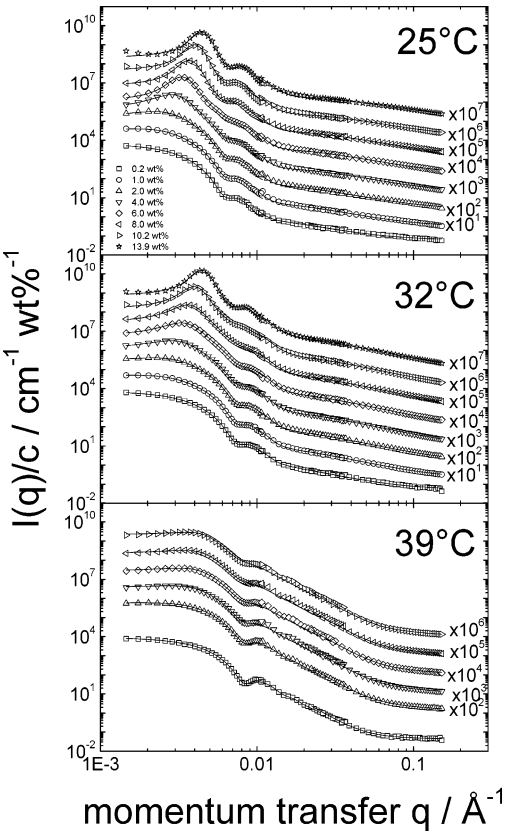

Figure 4. Intensity distribution normalized on concentration, $I(q)/c$, versus momentum transfer q for various concentrations of the M-5.5/115 microgel at 25, 32, and 39 °C. For the sake of clarity, some of the data sets were multiplied by constant factors as indicated. The lines represent fits according to eq 10.

In the intermediate q range (ca. $0.0055 < q < 0.03$ Å^{-1}), the main contribution to the overall scattering intensity $I(q)$ arises from the form factor $P_{\text{inho}}(q)$. Changes of the course of the scattering profiles as well as a shift of the form factor minimum toward higher q values are observed with increasing concentration (Figures 3 and 4). This indicates the compression of the particles at high concentrations. In contrast to rigid hard spheres, the particle form factor $P_{\text{inho}}(q)$ of the swollen PNiPAM microgel spheres obviously depends on concentration.

Figure 5 compares the structure factor $S(q)$ obtained by two different methods: the lines represent the structure factor $S(q)$ obtained from the direct modeling and, thus, taking the concentration dependence of the form factor $P_{\text{inho}}(q)$ into account by performing simultaneously a free fit of $P_{\text{inho}}(q)$ and $S(q)$. It should be noted that the quality of the fits is very good (see, for example, Figure 4). The fits obtained by the full fitting procedure have reduced χ^2 values in the range of $5 < \chi^2 < 50$. Therefore, the structure factors $S(q)$ derived by this procedure are quite reliable. In Figure 5, the symbols denote the structure factor $S(q)$ obtained by dividing the normalized scattering intensity distribution of a concentrated sample by the profile of a dilute sample $[I_{\text{conc}}(q)/c_{\text{conc}}]/[I_{\text{dil}}(q)/c_{\text{dil}}]$ assuming that the particle form factor $P_{\text{inho}}(q)$ remains unchanged with concentration. At 25 °C, the differences between the structure factors $S(q)$ obtained from the fitting procedure and the division of the experimental intensity distributions $[I_{\text{conc}}(q)/c_{\text{conc}}]/[I_{\text{dil}}(q)/c_{\text{dil}}]$ are fairly small. In contrast, at 32 °C significant deviations between the structure factors $S(q)$ obtained by the two approaches are observed. At 32 °C, the second peak of $S(q)$ obtained by the dividing procedure is even higher than the first peak, clearly

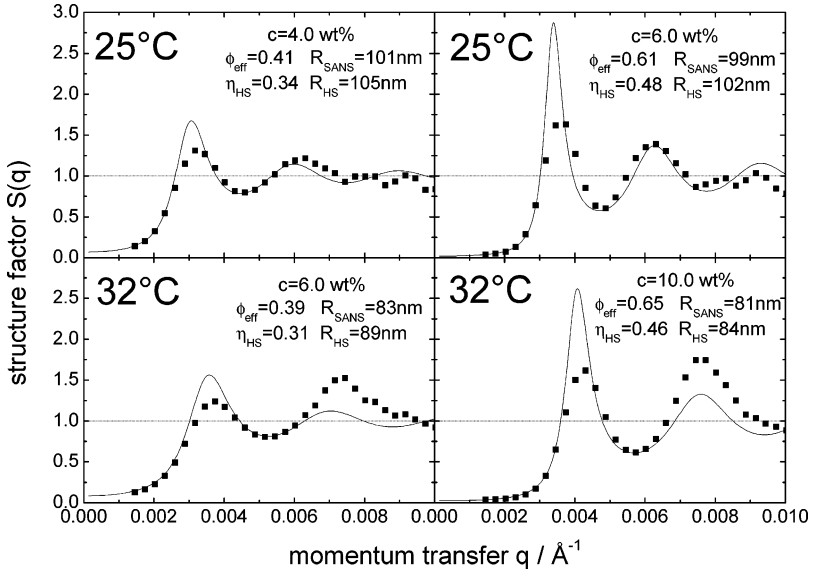

Figure 5. Comparison of the structure factor $S(q)$ obtained from the fitting procedure (line) taking the concentration dependence of the form factor $P_{inho}(q)$ into account and obtained by division of $[I_{conc}(q)/c_{conc}]/[I_{dil}(q)/c_{dil}]$ assuming a concentration-independent $P_{inho}(q)$ (symbols).

indicating the error made by neglecting the concentration dependence of the form factor.

The cross-linking density of the PNiPAM particles decreases gradually with increasing distance to the particle center. The elasticity of the polymer network is expected to be smaller at the outer regions of the particle than at the inner. Therefore, the outer regions can be compressed easier. An estimate of the relative contributions of the less cross-linked outer regions to the overall particle size is provided by the ratio of the width of the smeared particle surface σ_{surf} to the overall particle size R_{SANS}. When the temperature is altered from 25 to 32 °C, a slight increase of σ_{surf}/R_{SANS} is observed.[17] Hence, the compression of the particles is more efficient at the higher temperature. When a concentration-independent particle form factor $P_{inho}(q)$ is assumed, the compression of the particles is entirely neglected. The resulting error in the calculation of the structure factor $S(q)$ according to $[I_{conc}(q)/c_{conc}]/[I_{dil}(q)/c_{dil}]$ is, thus, larger at 32 °C than at 25 °C, which is in good agreement with the data shown in Figure 5.

Next, the high q regime (ca. $0.03 < q < 0.16$ Å^{-1}) will be discussed where the main contribution to the overall scattering intensity arises from concentration fluctuations of the polymer network that can be described by a Lorentzian (eq 8). The correlation length ξ can be considered to be related to the blob size describing the ensemble average correlations of the polymer network. As a result of the high incoherent background and the rather large statistical error of the experimental data in the high q regime, it was not possible to obtain ξ from dilute PNiPAM suspensions with high accuracy.[17,39,40] However, the statistics of the SANS data discussed in the present work was significantly better because the samples were more concentrated. The correlation length ξ was obtained reliably from the fitting procedure, and the effective volume fraction ϕ_{eff} dependence of ξ for the M-5.5/115 microgel at 25 °C can be seen in Figure 6. A decrease of ξ is observed with increasing effective volume fraction ϕ_{eff}. Thus, the network fluctuations are restricted to

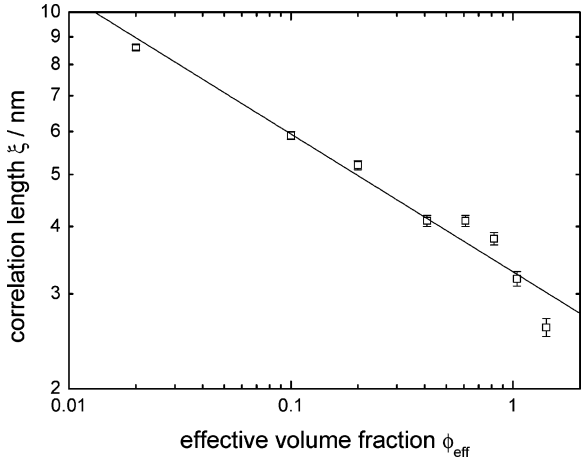

Figure 6. Correlation length of the network fluctuations ξ versus effective volume fraction ϕ_{eff} for the M-5.5/115 microgel at 25 °C. A power law behavior is observed, $\xi \propto \phi_{eff}^{-0.26}$.

smaller length scales at high effective volume fractions ϕ_{eff}. Our results are in good agreement with the small-angle X-ray scattering study of Ballauff et al. employing polystyrene-core-PNiPAM-shell particles.[40] They observed a similar decrease of the correlation length ξ with increasing temperature and a direct correlation of ξ and the temperature-dependent degree of swelling as expressed through the volume fraction. Apparently, the observed compression of the particle with increasing concentration also leads to changes in the internal network structure, indicating that the entire particle is compressed and not only the fuzzy surface.

The normalized scattering intensity distributions $I(q)/c$ of the larger particles M-1.5/353 obtained at various concentrations and temperatures are shown in Figure 7. Both the form factor minima and the structure factor peaks are shifted toward lower q values as compared to the M-5.5/115 sample, which has a higher degree of cross-linking density and smaller particle size.

The thermoresponsive PNiPAM particles shrink when the temperature is raised. The temperature induced deswelling leads to a decrease of the effective volume fraction ϕ_{eff} while the mass concentration c and the particle number density n is not changed. By the temperature

(39) Dingenouts, N.; Seelenmeyer, S.; Deike, I.; Rosenfeldt, S.; Ballauff, M.; Lindner, P.; Narayanan, T. *Phys. Chem. Chem. Phys.* **2001**, *3*, 1169.

(40) Seelenmeyer, S.; Deike, I.; Rosenfeldt, S.; Ballauff, M.; Lindner, P.; Narayanan, T. *J. Chem. Phys.* **2001**, *114*, 10471.

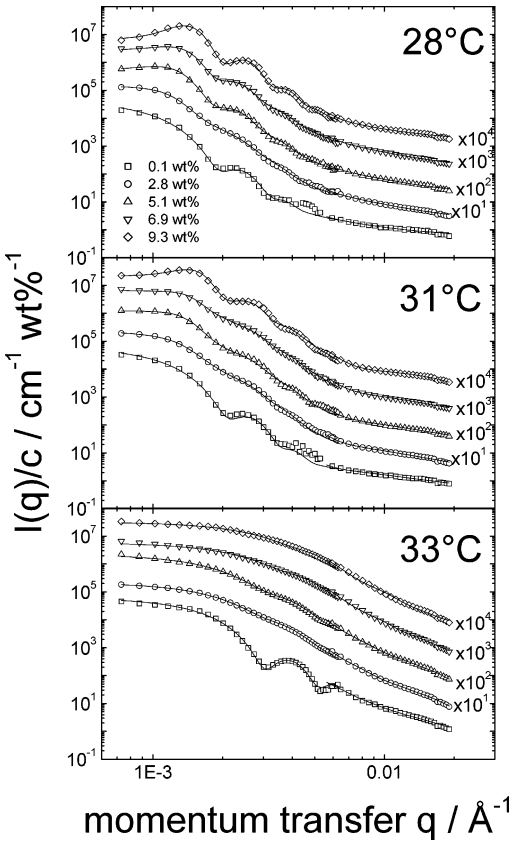

Figure 7. Intensity distribution normalized on concentration, $I(q)/c$, versus momentum transfer q for various concentrations of the M-1.5/353 microgel at 28, 31, and 33 °C. For the sake of clarity, some of the data sets were multiplied by constant factors as indicated. The lines represent fits according to eq 10.

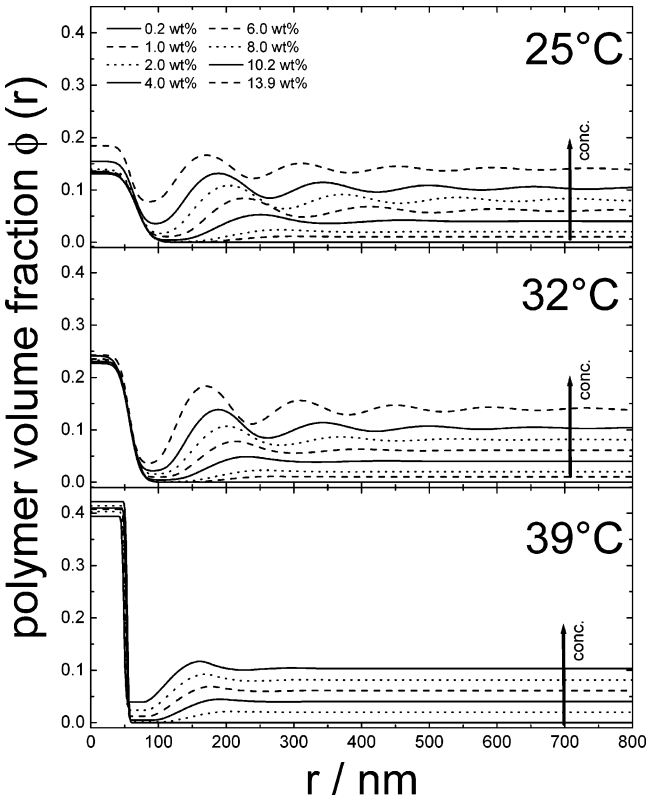

Figure 8. Radial polymer volume fraction profiles $\phi(r)$ for different concentrations of M-5.5/115 at 25, 32, and 39 °C.

variation, scattering profiles $I(q)/c$ obtained at different effective volume fractions ϕ_{eff} can be compared without changing the concentration c. When the temperature is raised, the form factor minima shift to higher q values for the M-5.5/115 and M-1.5/353 microgel (Figures 4 and 7). In contrast, the position of the structure factor peak remains unchanged upon heating at a given concentration c. The shift of the form factor minima indicates the temperature induced shrinkage of an individual particle whereas the unchanged position of the structure factor peak demonstrates that the average particle−particle distance is not altered. The center-to-center distance between different particles depends only on the particle number density n but is independent of the size of an individual particle.

The real space structures of the M-5.5/115 microgel at different concentrations and temperatures are revealed by the polymer volume fraction profiles $\phi(r)$, which are shown in Figure 8. The higher the concentration, the more maxima in the density profiles $\phi(r)$ are observed. The maxima in $\phi(r)$ indicate the position of the surrounding neighbors of a particle. The shift of the position of the maxima in the polymer volume fraction profiles $\phi(r)$ to smaller distances r clearly reveals the increasing compression of the particles with increasing concentration. At high concentrations, the volume fraction profiles $\phi(r)$ do not approach 0 anymore, indicating the increasing overlap of the particles. A certain volume fraction of the polymer constitute a homogeneous component ϕ_{homo} that spans the entire sample. The polymer volume fraction in the center of a particle $\phi(0)$ increases slightly with concentration. The overlap of the particles is restricted to the outer regions of the sphere, which exhibit a lower degree of cross-linking density. The inner regions of the particle, which are characterized by the box profiles up to a distance of R_{box}, do not interpenetrate. At large distances r, the density profiles $\phi(r)$ approach the average polymer volume fraction that is given by the mass concentration.

With increasing temperature, the polymer volume fraction in the center of the particle $\phi(0)$ increases significantly. The observation of well-defined maxima in the density profiles $\phi(r)$ at 32 °C reveal a long-ranged ordered structure, although the temperature is only approximately 1 K below the LCST.

To obtain information about temperature-induced changes in the interaction potential, Figure 9 compares the normalized polymer volume fraction profiles $\phi(r)/c$ versus $r/R_{SANS(dilute)}$ at different temperatures for similar effective volume fractions ϕ_{eff}. The normalized polymer volume fraction profiles $\phi(r)/c$ at 25 and 32 °C coincide on a single curve for all effective volume fractions ϕ_{eff}. The structure formation depends only on the effective volume fraction ϕ_{eff}. Thus, the particle−particle interaction potential does not change significantly between 25 and 32 °C. Even approximately 1 K below the LCST, the experimental scattering intensity distributions $I(q)/c$ are described very well by the hard sphere structure factor $S(q)$ (see Figure 4). This might indicate that the interaction potential is still repulsive at 32 °C. An attractive interaction potential would eventually lead to aggregation of the particles, giving rise to an increase of the scattering intensity $I(q)/c$ in the very low q regime ($0.001\ Å^{-1} < q$), which was not investigated in our experiments.

As mentioned previously (section IV.A), concentrated suspensions of the M-1.4/141 microgel form colloidal crystals. The temperature-induced phase transition from a colloidal crystal to a liquid was investigated by SANS, and the normalized intensity distributions $I(q)/c$ are shown in Figure 10. First-, second-, and third-order Bragg peaks are observed at 26 °C, indicating a highly ordered crystal

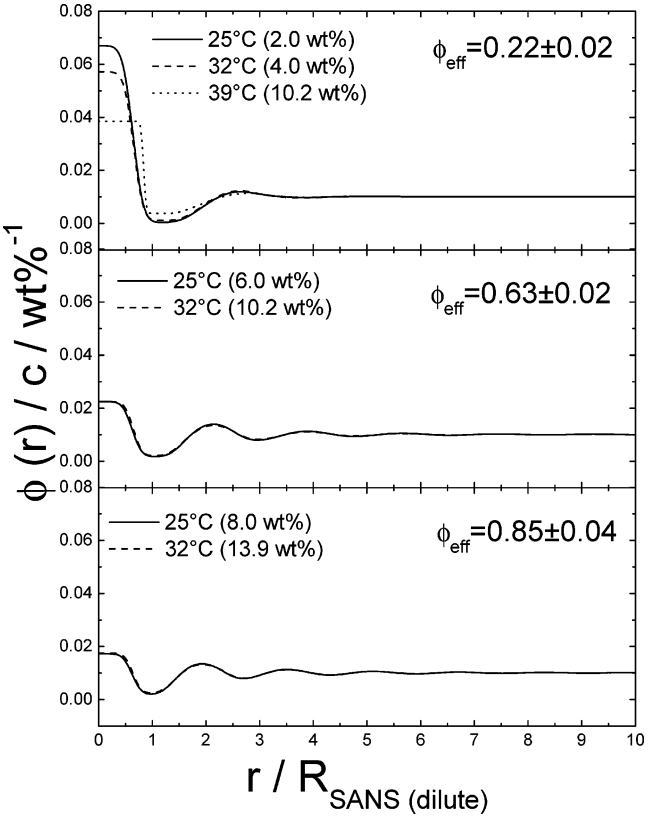

Figure 9. Normalized radial polymer volume fraction profiles, $\phi(r)/c$, versus $r/R_{SANS(dilute)}$ for M-5.5/115 at 25 and 32 °C for similar volume fractions but different concentrations.

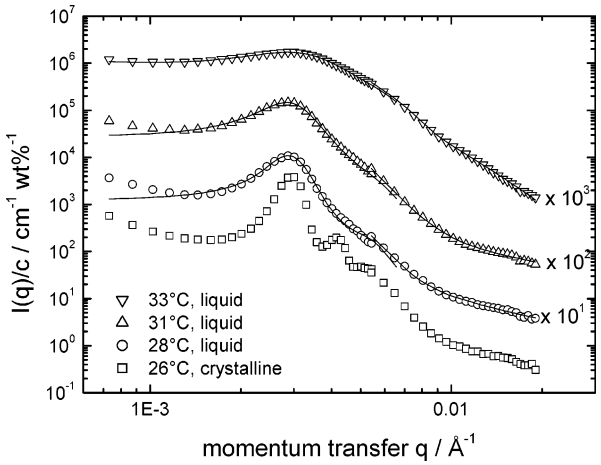

Figure 10. Temperature induced crystalline-liquid-phase transition for M-1.4/141 at a concentration of $c = 3.6$ wt % seen by SANS. The lines represent fits according to eq 10.

lattice structure. Upon heating, the effective volume fraction ϕ_{eff} decreases and the crystal melts. The Bragg peaks of higher order vanish but, again, the position of the structure factor peak does not change with temperature because the particle number density n was not altered.

C. Structure Formation at Temperatures above the LCST. At temperatures above the LCST, macroscopic phase separation occurs in concentrated PNiPAM microgel suspensions. The structure factor peaks, which were observed for the M-5.5/115 and M-1.5/353 microgel at temperatures below the LCST, almost vanished for all concentrations at 39 °C (Figures 4 and 7). The corresponding polymer volume fraction profiles $\phi(r)$ obtained for the M-5.5/115 at 39 °C are shown in Figure 8. The

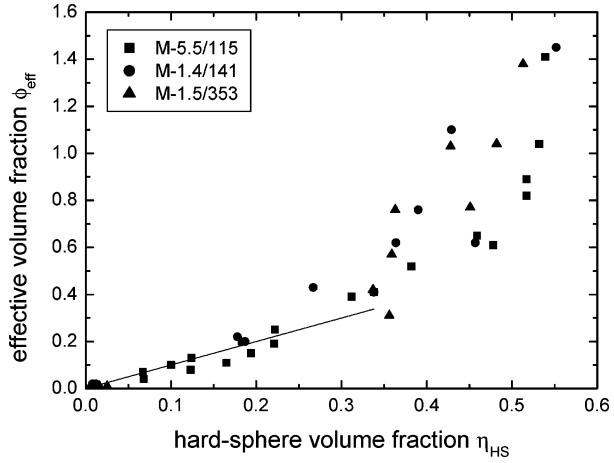

Figure 11. Effective volume fraction ϕ_{eff} versus hard sphere volume fraction η_{HS} for all microgels at all temperatures. The line represents hard sphere behavior ($\phi_{eff} = \eta_{HS}$).

polymer volume fraction in the center of a particle $\phi(0)$ is almost independent of concentration, and even in the collapsed state, the particles still contain more than 55% water. The particle surface sharpened dramatically compared to temperatures below the LCST. Only one broad maximum is observed in the density profiles $\phi(r)$ at high concentrations, indicating only one well-defined layer of surrounding neighbor particles. At 39 °C, which is well above the LCST, the collapsed particles have obviously formed a structure without any long-range order. The strongly attractive interaction potential led to an aggregation of the spheres, and these aggregates comprise polymer particles that are flocculated together and interpenetrate strongly. Actually, this effect is used for film formation in microgel-based polymer coatings. Thus, the structure formation of the PNiPAM microgels at temperatures above the LCST is distinctively different compared to that of attractive hard sphere colloids. An attractive interaction potential in suspensions of rigid hard spheres should not lead to random polymer-like flocs but to the formation of aggregates with a higher degree of long-range order.

D. Comparison of PNiPAM Microgels with Different Cross-Linking Densities and Particle Sizes. Figure 11 compares the effective volume fraction ϕ_{eff} obtained from viscometry in dilute solution with the hard sphere volume fraction η_{HS} determined from the fitting procedure of the experimental scattering curves. Data for the three microgels at various temperatures and concentrations are presented together with a line representing hard sphere behavior, for example, $\phi_{eff} = \eta_{HS}$. All microgels reveal hard sphere behavior up to $\phi_{eff} \approx 0.35$ independent of the cross-linking density or size. At higher effective volume fractions $\phi_{eff} > 0.35$, the softness of the particles is revealed and strong deviations from the hard sphere behavior occur. It should be noted again that the Percus−Yevick hard sphere model agrees with simulations of hard spheres up to volume fractions of about $\eta_{HS} \approx 0.45$. At higher volume fractions η_{HS}, the Percus−Yevick model is not expected to be valid, resulting in an underestimation of concentration effects. Thus, caution must be taken interpreting the results obtained from the fits of the highly concentrated samples.

The particle radius R_{SANS} determined from the fits of the form factor $P_{inho}(q)$ and the hard sphere radius R_{HS} obtained from the structure factor $S(q)$ fit are displayed as a function of the effective volume fraction ϕ_{eff} in Figure 12 for the M-5.5/115 and M-1.4/141 microgels. At all temperatures, a gradual decrease of both R_{SANS} and R_{HS}

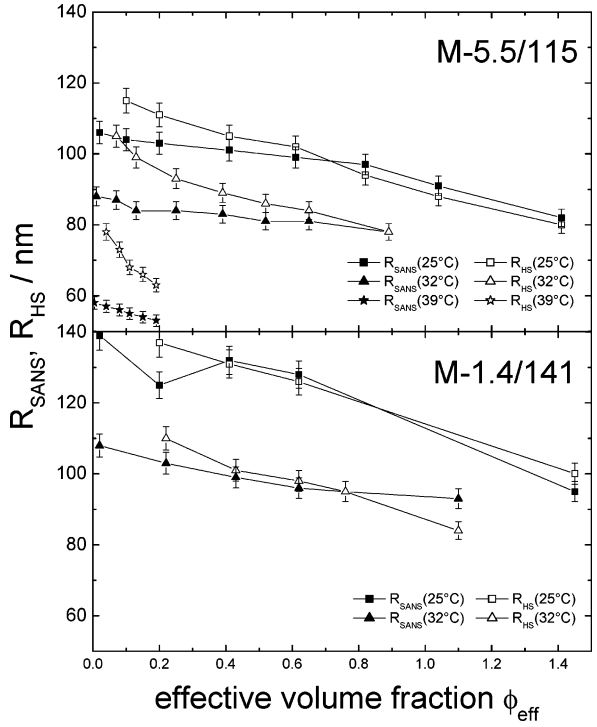

Figure 12. Radii obtained from the analysis of the form factor R_{SANS} and structure factor R_{HS} versus effective volume fraction ϕ_{eff} for the M-5.5/115 and M-1.4/141 microgels.

with increasing effective volume fraction ϕ_{eff} is observed. The strong decrease at high effective volume fractions ϕ_{eff} is caused by compression of the soft PNiPAM particles as discussed in section IV.B. Surprisingly, already at rather small effective volume fractions $\phi_{eff} < 0.35$ a decrease of both radii is observed that cannot be caused by interpenetration of the particles. This effect might be due to a form of excluded volume screening. For the individual particle, a slight shrinkage leads to a loss of configurational entropy of the polymer strands inside the particle. On the other hand, the microgel particle gains translational entropy. At higher concentrations, the overlap of the particles that we consider as part of a flat solvent background (see section III) will make the particles smaller even at small effective volume fractions ϕ_{eff}. In fact, the particle is considered only to be the contribution that is above the background.

V. Conclusions

We address the question whether thermoresponsive PNiPAM microgels can be used as model systems for concentrated colloidal suspensions. A previously described model expression for the particle form factor $P_{inho}(q)$ is extended by a model hard sphere structure factor $S(q)$ to describe experimental data at a high concentration. The particle form factor $P_{inho}(q)$ accounts for the inhomogeneous distribution of the polymer segment density throughout an individual particle, whereas the Percus−Yevick hard sphere structure factor $S(q)$ describes the correlations between different particles. Average radial density profiles $\phi(r)$ are calculated from the amplitude of the form factor $A(q)$ and the structure factor $S(q)$. By this procedure, a direct real space description of the spatial ordering in the neighborhood of a single particle is obtained. The model expression describes the experimental scattering intensity distributions $I(q)$ very well over the entire q regime for a broad range of concentrations at temperatures below as well as above the LCST. The main conclusions are the following:

(a) The overall particle size and the correlation length ξ of the concentration fluctuations of the internal polymer network decrease with concentration revealing the increasing compression of the spheres. In contrast to suspensions of rigid hard spheres, the concentration dependence of the particle form factor $P_{inho}(q)$ of the swollen PNiPAM microgels needs to be accounted for when structure factors $S(q)$ of concentrated suspensions are discussed. Senff and Richtering already showed that the particles are compressed in the crystalline and glassy regions.[18] Our present results demonstrate that the particle size changes already in the liquid regime.

(b) The particle−particle interaction potential does not change significantly between 25 and 32 °C. Even approximately 1 K below the LCST, the experimental scattering intensity distributions $I(q)/c$ are described very well by the hard sphere structure factor $S(q)$ by using an equivalent hard sphere particle size R_{HS} and volume fraction η_{HS}. The hard sphere parameters $R_{HS}(c)$ and $\eta_{HS}(c)$ differ from R_{SANS} and the effective volume fraction ϕ_{eff}. At 39 °C, which is well above the LCST, the interaction potential becomes strongly attractive leading to macroscopic phase separation. The collapsed microgel spheres form aggregates consisting of flocculated particles without significant long-range order. Instead, only one well-defined layer of surrounding neighbor particles is observed. Hence, an attractive interaction potential in concentrated suspensions of PNiPAM microgels leads to distinctively different structures as compared to attractive hard sphere colloids.

(c) As mentioned above, concentrated suspensions of PNiPAM microgel particles can be described within the framework of a hard sphere structure factor $S(q)$ when equivalent hard sphere parameters R_{HS} and η_{HS} are employed. Microgels with different degrees of cross-linking and particle size resemble true hard sphere behavior up to effective volume fractions of $\phi_{eff} < 0.35$. At higher effective volume fractions $\phi_{eff} > 0.35$, strong deviations from true hard spheres are observed. Interpenetration of the outer and less cross-linked regions of the soft spheres as well as particle compression occur at higher concentrations. The equilibrium colloidal phase behavior also reveals a soft sphere behavior as indicated by the shift of the freezing transition ϕ_f toward higher effective volume fractions. The divergence of the relative zero shear viscosity $\eta_{0,rel}$ occurs at higher effective volume fractions ϕ_{eff} as well, and the power law concentration dependence of the plateau modulus G_P reveals typical soft sphere behavior.

Thermoresponsive PNiPAM microgels can be considered a model system in colloidal science when the properties just mentioned are taken into account. The temperature sensitivity leads to several advantages over other systems: (i) The preparation of concentrated samples at low temperatures is facilitated because the suspensions can be prepared at elevated temperatures with low viscosity and cooling will lead to homogeneous particle swelling. (ii) The liquid−solid transition (crystallization and glass transition) can be investigated both as a function of concentration at constant temperature and as a function of temperature at a constant particle number density. (iii) The aggregation behavior near the LCST can be used to study the onset of film formation.

Acknowledgment. Financial support by the Deutsche Forschungsgemeinschaft and the Danish Natural Science Research Council is gratefully acknowledged.

LA049518X